Chinese Chemical Letters 31 (2020) 2007–2012

Contents lists available at ScienceDirect

Chinese Chemical Letters

journal homepage: www.elsevier.com/locate/cclet

Communication

ZIF-67 derived hollow Ni-Co-Se nano-polyhedrons for flexible hybrid supercapacitors with remarkable electrochemical performances

Guangmeng Qu[a], Xixi Zhang[a], Guotao Xiang[a], Yunrui Wei[a], Jiangmei Yin[a], Zonghua Wang[a], Xiaoli Zhang[b], Xijin Xu[a,*]

[a] School of Physics and Technology, University of Jinan, Ji'Nan 250022, China
[b] State Centre for International Cooperation on Designer Low-Carbon & Environmental Materials, School of Materials Science and Engineering, Zhengzhou University, Zhengzhou 450001, China

ARTICLE INFO

Article history:
Received 26 December 2019
Received in revised form 16 January 2020
Accepted 19 January 2020
Available online 20 January 2020

Keywords:
Ni-Co-Se
Nano-polyhedrons
Hybrid supercapacitors

ABSTRACT

Nano-polyhedral $NiSe_2/CoSe_2$ (Ni-Co-Se) with hollow architectures are synthesized by selenizing the precursors of Ni-Co bimetallic hydroxides that are directly derived from ZIF-67. The as-fabricated Ni-Co-Se electrodes exhibit high specific capacitance of 1668 F/g at 1 A/g accompanying with outstanding rate capability (about 82.8% retention of the initial capacity at 20 A/g). The corresponding Ni-Co-Se//AC all-solid-state hybrid supercapacitors are assembled by directly using the Ni-Co-Se on carbon fabric as the positive electrode, which deliver high energy density and power density (38.5 Wh/kg at 802.1 W/kg, 32.0 Wh/kg at 8008.8 W/kg), excellent cyclic stability (82.3% retention after 5000 cycle) and robust mechanical flexibility (no obvious attenuation at bending to different angles). This work will provide a new and smart route for constructing transition metal selenides for supercapacitor devices.

With the rapid development of new sustainable energy industries (solar energy, wind energy, hydrogen energy, *etc.*), reliable storage equipment for efficient conversion between new energy and electric energy have grown a tremendous demand in the current society [1–3]. Among numerous new conversion/energy storage devices, supercapacitor, also known as electrochemical capacitor, has become one of the most promising candidates for the next generation energy storage system with its fast charging, remarkable cycle stability, conspicuous high power density and environment-friendly characteristics [4–6]. Although available supercapacitors have been in a position to deliver a desired specific capacitance compared with traditional solid-state electrolytic capacitors, they still suffer from lower energy density than rechargeable batteries [7–10]. Consequently, without sacrificing the power density and cycle stability, reasonable and effective amelioration of the energy density of supercapacitor will be the research tendencies. As the vital component of supercapacitors, electrode materials play a decisive role in the energy density and chemical stability of the device [9,11–13]. Therefore, it is highly desirable to explore trustworthy electrode materials with conspicuous architecture and performances for supercapacitors.

On the way to searching adequate supercapacitor electrode materials with remarkable electrochemistry properties, extensive research efforts are underway, mainly containing optimizing the conductivities [14,15], constructing microstructures [1,16–18] and exchanging/storing more than one electron at each faradic redox reaction center [19,20], *etc.* Rencently, ternary transition metal chalcogenides, such as $NiCo_2S_4$ [21], $NiFeS_2$ [22], $CoMoS_4$ [23] and $NiMoS_4$ [24] have received extensive research interest owing to higher electrochemical activity, shorter electron/ion transport lengths and richer redox reactions. However, low conductivity and poor stability place restriction on their electrochemical performance further improvement. Compared with sulfides, selenides hold higher conductivity and electrochemical activity, because of their faster reaction kinetics (1×10^{-5} S/m) and weaker electronegativity (2.4) [25,26], which signifies that transition metal selenides will be the satisfactory candidates of electrode material for supercapacitor. Furthermore, the reasonable design of micro-nano structure is also an effective strategy to ensure the excellent electrochemical performance of electrode materials. Hollow nanomaterials with interior cavities and functional shells boundaries exhibit vast prospects in the application of supercapacitor electrode materials by virtue of their remarkable merits such as shortened charge transport paths, low density, high surface to

* Corresponding author.
E-mail address: sps_xuxj@ujn.edu.cn (X. Xu).

https://doi.org/10.1016/j.cclet.2020.01.040
1001-8417/

volume ratio, and kinetically favorable open structure [17,25,27]. MOFs are an organic-inorganic hybrid material with periodic network structure, which are composed of organic ligands and metal ions/clusters by self-assembly of coordination bonds [28]. They have well-defined pore size, controllable shape and high specific surface area, and are identified as an ideal sacrificial template to fabricate hollow transition metal compounds in recent years [28,29]. Many studies have been reported on the use of MOFs derived hollow nanostructures for supercapacitor electrodes. For example, Wang *et al.* [30] employed ZIF-67 MOFs as a template to synthesize amorphous $CoNi_2S_4$ nanocages by hydrothermal and sacrifice template method, which displayed the high specific capacitance of 1890 F/g at 4 A/g, and excellent cycle stability (the capacitance retention of 71% after 5000 cycling charge-discharge measurements at 10A/g). Yang *et al.* [31] using Ni/Co-based MOFs as template by hydrothermal method, derived the core-shells $NiCo_2O_4$/NiO structure on Ni foam, which delivered specific capacitance of 726 F/g at 1 A/g with and excellent rate capability (the capacitance retention of 84% at 20 A/g). However, at present, the design and fabrication of MOFs-derived, the transition metal selenides for supercapacitor electrodes have rarely been reported.

In this work, we report an electrode material of hollow $NiSe_2/CoSe_2$ bimetallic selenide for supercapacitor, which is designed and constructed by using ZIF-67 synthesized in classical experiments as a template. This designed strategy comprises of the synthesis of ZIF-67 dodecahedron, cation-exchange with a Ni^{2+} and selenization employing solution of selenium sodium hydride (NaHSe). The hollow nano-polyhedral structure takes full advantages of the synergies between $NiSe_2$ and $CoSe_2$ to integrate a range of components and structural merits, involving sufficient electroactive sites, large specific surface areas and accelerated ion/electron diffusion and transport, which endow Ni-Co-Se electrodes prominent electrochemical energy storage performance. Meanwhile, the as-assembled hybrid supercapacitor with Ni-Co-Se as a positive electrode exhibits a high energy density of 38.5 Wh/kg at 802.1 W/kg, extraordinary cyclic lifespan (about 82.3% retention after 5000 cycles), and robust mechanical flexibility.

All the chemicals are analytical grade without additional purification. Nickel nitrate hexahydrate ($Ni(NO_3)_2{\cdot}6H_2O$), 2-methylimidazole ($CH_3C_3H_3N_2$) and polyvinyl alcohol (PVA) are purchased from Aladdin Reagent Inc. Corporation (Shanghai, China), and others are purchased from Sinopharma. According to previously reported methods, the ZIF-67 polyhedrons are synthesized in a typical procedure [32]. Firstly, 4 mmol $CH_3C_3H_3N_2$ was added to a solution of 2 mmol cobalt nitrate ($Co(NO_3)_2{\cdot}6H_2O$) in 20 mL of methanol, and stirring was kept for 1 h to form a homogeneous suspension solution. Afterwards, the obtained homogeneous mixture solution was remained at 25 °C for 24 h. The violet product was cleaned repeatedly with methanol for several times, collected by centrifugation and dried under a vacuum of 60 °C for 12 h to form ZIF-67 powder. The NaHSe solution was prepared by mixing stoichiometric sodium borohydride, selenium powder and deoxygenated DI water under nitrogen protection based on the following equation: $4NaBH + Se + 7H_2O = 2NaHSe + Na_2B_4O_7 + 14H_2$ [33].

Synthetic ZIF-67 and fresh NaHSe solution were used as precursors and selenium sources to prepare Ni-Co-Se nano-polyhedrons by cation exchange and sacrificial template method. In detail, 74 mg ZIF-67 powder was ultrasonically dispersed into 50 mL 0.01 mol/L $Ni(NO_3)_2{\cdot}6H_2O$ alcohol solution. The mixture was continuously stirred for 30 min, then the precipitate was collected by centrifugation and dried in a vacuum of 60 °C for 12 h. After that, the resulting product was dispersed into 35 mL of deionized water, and the 5 mL 0.5 mol/L NaHSe solution was added and stirring was continued for 30 min to obtain a dark gray solution, which was then transferred to a 50 mL stainless steel autoclave. The reaction equipment is maintained at 100 °C for 6 h, followed by naturally cooling to ambient temperature. Finally, the precipitate was cleaned with alcohol and DI water and dried in a vacuum of 60 °C to obtain Ni-Co-Se nano-polyhedrons. To serve as experimental control, the Co-Se and Ni-Co-O nano-polyhedrons were synthesized *via* removing the procedure of adding $Ni(NO_3)_2{\cdot}6H_2O$ and annealing cation exchange products directly in air (300 °C, 3 h), respectively.

Scanning electron microscopy (SEM) images are detected using a field emission scanning electron microscope (FESEM, FEI QUANTA FEG250). The crystal morphologies, chemical compositions, phases and chemical valence states are investigated by transmission electron microscope (TEM, FEI Tecnai G2 F20), equipped with an energy dispersive X-ray spectrometer (EDS), XRD (D8-Advance Bruker) and a X-ray photoelectron spectroscopy (XPS, Thermo ESCALAB250Xi). The electrochemical performance of the electrode materials is evaluated in a three electrode configuration consisting of a working electrode, a platinum pair electrode and a Hg/HgO reference electrode using an electrochemical workstation, wherein the working electrode was prepared by uniformly mixing electrode materials, polyvinylidene fluoride (PVDF) and acetylene black (8:1:1) loading on a carbon fabric. Measurements of cyclic voltammetry (CV), galvanostatic charge-discharge (GCD) and electrochemical impedance spectroscopy (EIS) are performed on CHI660E electrochemical workstation and Autolab PGSTAT 302 N adopting a 3 mol/L KOH aqueous solution as the electrolyte. The capacitance of the synthesized materials is calculated from the results of as-measured GCD curve by the following formula [34]:

$$C = \frac{I\Delta t}{\mathrm{A}} \tag{1}$$

where C (F/g) represents the specific capacity, I (A) and Δt (s) are charge/discharge current and current time in the discharge process, A is mass loading of active electrode material loading on the carbon fabric about 2 mg/cm^2.

The flexible hybrid supercapacitor is assembled with Ni-Co-Se positive electrode, activated carbon (AC) negative electrode and PVA-KOH gel electrolyte, in which the AC and Ni-Co-Se electrode is made by evenly coating the carbon fabric with a mixture of 1 mL *N*-methylpyrrolidinone (NMP), 10 mg acetylene black, 80 mg AC or Ni-Co-Se and 10 mg PVDF slurry. The PVA-KOH solid electrolyte-separator films is obtained by dispersing 6 g KOH and 6 g PVA in 60 mL DI water heated to 90 °C under stirring for 2 h. The specific capacitance of flexible asymmetric supercapacitor can be calculated based on the discharge time in GCD curve of two-electrode measurements according to the following formula [20]:

$$C = \frac{I\Delta t}{VA} \tag{2}$$

where C (F/g) is the specific capacitance, I (A) and Δt (s) are current and time of discharge process, V (V) refers to the operating voltage window and A is the total mass of the Ni-Co-Se and AC loading on carbon fabric.

The power density and energy density can be calculated according to following formulas [7,35]:

$$E = \frac{1}{2}CV^2 \tag{3}$$

$$P = \frac{E}{\Delta t} \tag{4}$$

where E (Wh/kg) and P (W/kg) are energy density and power density, C (F/g), V (V) and Δt (h) are specific capacitance, voltage window and discharge time of as-assembled supercapacitor, respectively.

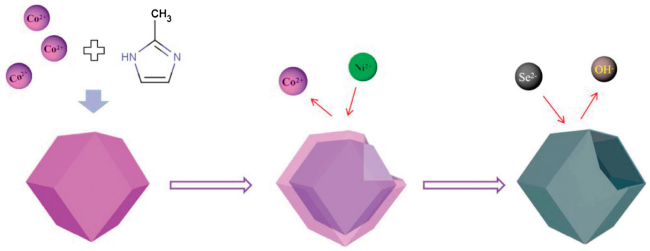

Fig. 1. Schematic synthesis process of hollow Ni-Co-Se nano-polyhedras.

The schematic synthesis process of hollow Ni-Co-Se nano-polyhedrons is illustrated in Fig. 1. $Co(NO_3)_2{\cdot}6H_2O$ and $CH_3C_3H_3N_2$ are used as Co^{2+} source and organic ligand to synthesize the ZIF-67 precursor. After that, a classical anion exchange process is performed. During this process, Ni^{2+} (from adding $Ni(NO_3)_2{\cdot}6H_2O$) in the solution is hydrolyzed to produce protons and slowly etch the ZIF-67 polyhedron, which will lead to the precipitation of Co ions. The precipitated Co ions and the external Ni^{2+} co-deposited on the surfaces of the nano-polyhedron to form Ni-Co double hydroxides [36]. Finally, the Ni-Co double hydroxides are successfully converted into the hollow Ni-Co-Se nano-polyhedrons *via* a selenation and further etching reaction using NaHSe in a high temperature hydrothermal environment.

Fig. 2a clearly shows that the synthesized ZIF-67 templates present a classic rhomboid dodecahedron with regular facets, well defined corners and smooth surfaces, which accurately correspond to the symmetry and self-limitation of ZIF-67. Ni-Co double hydroxides after Ni^{2+} exchange are depicted in Fig. 2b. The shape of the polyhedron is well maintained, while the surfaces become rough due to co-deposition of Ni-Co double-hydroxide on the surfaces. After selenation reaction, the hollow Ni-Co-Se nano-polyhedron is constructed as shown in Fig. 2c. As a reference, the SEM images of Co-Se and Ni-Co-O are shown in Fig. S1 (Supporting information).

TEM image in Fig. 2d shows that the diameter of the Ni-Co-Se polyhedron with clear hollow structure is about 650 nm, and the thickness of the outer shell is about 50 nm (determined by the dark

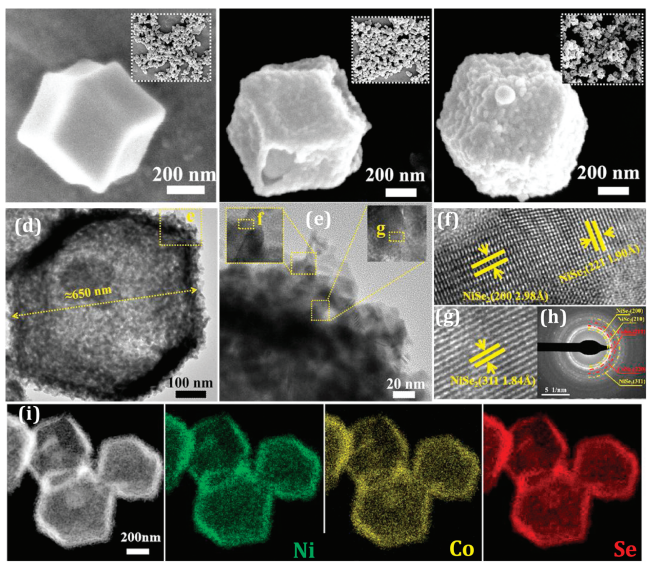

Fig. 2. SEM images of ZIF-67 (a), Ni-Co double hydroxides (b) and Ni-Co-Se nano-polyhedron (c); TEM images (d) and HRTEM (e–g) of Ni-Co-Se nano-polyhedrons; (h) SAED diffraction image of Ni-Co-Se nano-polyhedrons. (i) The EDX mapping of Ni-Co-Se nano-polyhedras for Ni, Co, Se elements.

areas at the edges), which well corresponds to the information in the SEM image. Moreover, the surfaces of Ni-Co-Se nano-polyhedron are loaded with a mass of nanoparticles and nano-sheets, which provides abundant interspaces to facilitate the transport and infiltration of electrolyte expediting ion/electron transfer reactions. The area selected from the dotted portion is magnified in the HRTEM image in Figs. 2e-g, where the well-ordered crystalline lattice of 2.98 Å, 1.90 Å and 1.84 Å are accurately indexed the (200), (221) plane of $NiSe_2$ and the (311) plane of $CoSe_2$, respectively [37,38]. Simultaneously, corresponding SAED diffraction image (Fig. 2h) with distinct circular diffraction spots indicates the polycrystalline feature of Ni-Co-Se nano-polyhedron and the circular diffraction spots are assigned to (211) and (220) planes of $CoSe_2$ and (200), (210), and (311) planes of $NiSe_2$ [39]. The elemental compositions of Ni-Co-Se are conformed by EDS spectrum (Fig. S2 in Supporting information), among which the C and O originate from adsorption to the air, and Cu from the loading holder [40]. As shown in Fig. 2i, the elements of Ni, Co, and Se are evenly distributed on the whole polyhedral shell, indicating the successful syntheses of the bimetallic selenides. The XRD pattern (Fig. S3 in Supporting information) is investigated to explore the crystalline structure of the Ni-Co-Se nano-polyhedron, where all diffraction peaks can be indexed well with the standard hexagonal $CoSe_2$ (PDF card No. 53-0449) and $NiSe_2$ (PDF card No. 18-0886), demonstrating the coexisting phase of $NiSe_2$ and $CoSe_2$ after selenylation reaction.

To further investigate element compositions and chemistry states of Ni-Co-Se, XPS analyses are performed. The full-survey XPS spectrum of Ni-Co-Se exhibited in Fig. 3a demonstrates the coexist of C, O, Co, Ni and Se elements, which are consistent with conclusions of XRD and EDS. The Ni 2p spectrum in Fig. 3b can be accurately fitted with two spin-orbit splittings of Ni $2p_{3/2}$ and Ni $2p_{1/2}$ accompanied by two concomitant shakeup satellites (indicated as "sat."), among which the fitting peaks with binding energies of 853.3/871.3, 855.6/874.7 and 860.5/879.5 eV, are assigned to Ni^{2+} and Ni^{3+}, respectively [16,41]. Similarly, the Co 2p in Fig. 3c, can be accurately fitted with two spin-orbit splitting of Co $2p_{3/2}$ and Co $2p_{1/2}$, where the fitting peaks with binding energies of 778.6/780.6, 793.6/797.0, and 784.7/802.1 eV are indexed to the characteristics of Co^{3+}, Co^{2+} and two "sat." signals, respectively [41,42]. The Se 3d spectrum of Ni-Co-Se are depicted in Fig. 3d, in which peaks at around 54.5 and 55.2 eV can be associated with Se $3d_{3/2}$ and Se $3d_{5/2}$ in low coordination and Metal-Se (Co-Se/Ni-Se) bonds. The peak with binding energies at 59.0 eV corresponds to SeO_x, which is originated from partial oxidation [42–44].

CV curves of Ni-Co-Se nano-polyhedron in Fig. 4a, display a pair of well-defined faradaic redox peaks located at 0-0.7 V, manifesting the occurrence of strong faradaic redox reactions of Ni-Co-Se especially at low sweep rates. These redox reactions correspond to the conversion Ni/Co–Se and Ni/Co–Se–OH during the energy storage process [42]. Meanwhile, the curve shapes and symmetry of redox peaks are well maintained with the increase of sweep rates indicating fast electronic and ionic transport, which endow Ni-Co-Se electrodes advantageous rate capability. The GCD profiles in Fig. 4c display that the time-potential correlation curves of Ni-Co-Se electrode are quasi-symmetric shapes with a pair of distinct potential plateaus, which reveal outstanding coulombic efficiency and pseudocapacitive behaviors originated from the highly reversible redox reactions of the electrode during process of charging/discharging [45].

For contrasts, the CV and GCD curves of Co-Se, Ni-Co-O, and Ni-Co-Se electrode are depicted in Fig. 4b and Fig. S4 (Supporting information). CV curves of Co-Se, Ni-Co-O and Ni-Co-Se in Fig. 4b show that the CV curve of Ni-Co-Se delivers a pair of stronger redox signal peaks and a larger curvilinear closed area compared with

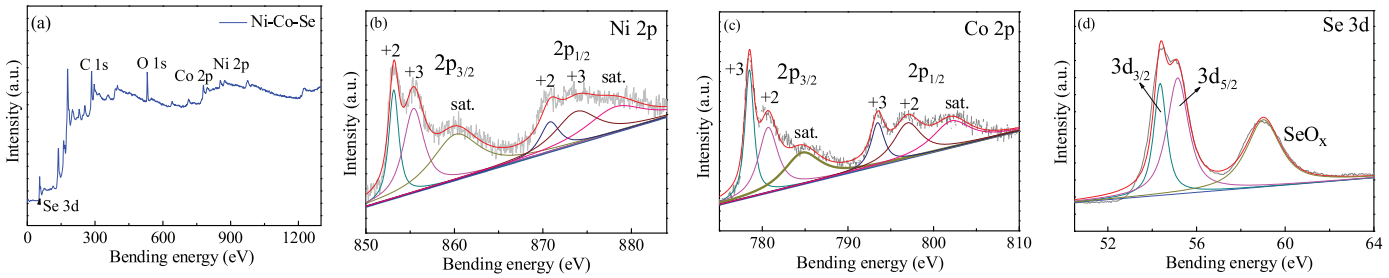

Fig. 3. XPS spectra of the Ni-Co-Se nano-polyhedrons: (a) Ni-Co-Se, (b) Ni 2p, (c) Co 2p, (d) Se 3d.

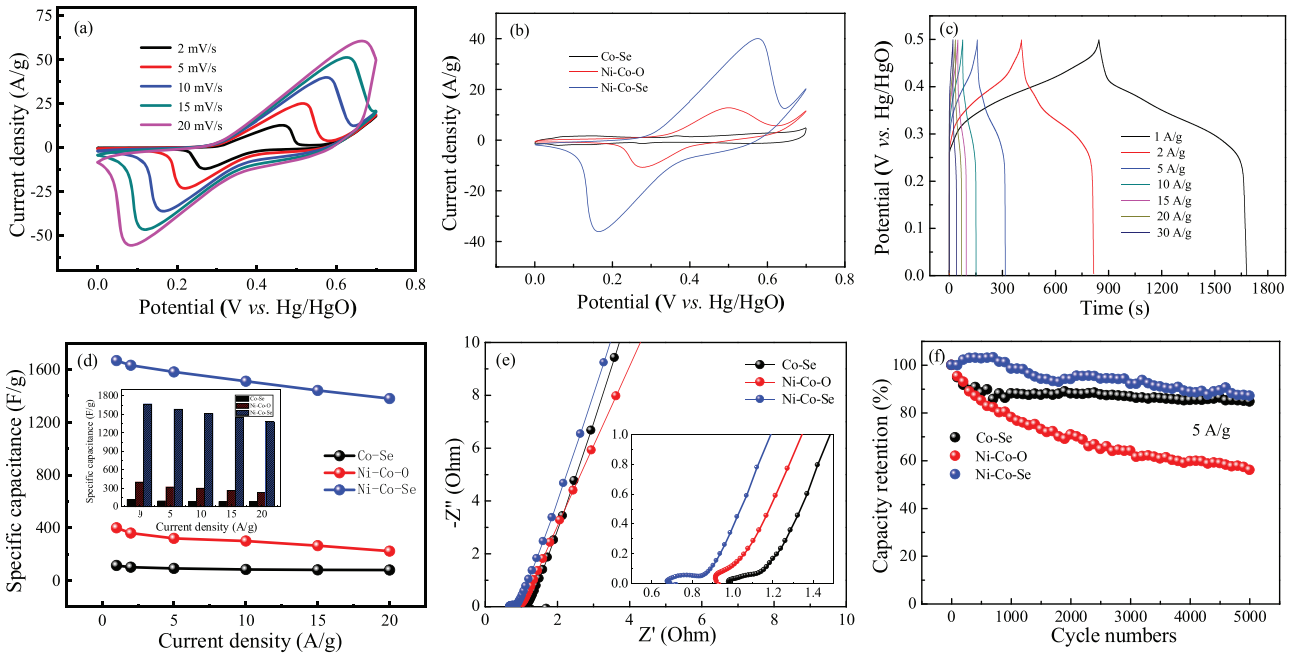

Fig. 4. (a) CV curves of the Ni-Co-Se electrode at different scanning rates from 2 mV/s to 20 mV/s. (b) CV curves of Co-Se, Ni-Co-O and Ni-Co-Se at 10 mV/s. (c) GCD curves of Ni-Co-Se electrode at different current densities from 1 A/g to 30 A/g. (d) Specific capacitances of Co-Se, Ni-Co-O and Ni-Co-Se. (e) EIS of Co-Se, Ni-Co-O and Ni-Co-Se. (f) Cycling performance of Co-Se, Ni-Co-O and Ni-Co-Se at the current density of 5 A/g.

Co-Se and Ni-Co-O, demonstrating that the capacitance and kinetic process of redox reaction of electrode is significantly optimized rooting from the double metal (Ni/Co) ions synergistic effect and the excellent electrical conductivity in the bimetallic selenides. The mass specific capacitances of as-fabricated Co-Se, Ni-Co-O and Ni-Co-Se electrode at current densities ranging from 1 A/g to 20 A/g are calculated according to the discharge time and potential in the GCD curve. As shown in Fig. 4d, compared with Co-Se and Ni-Co-O, the Ni-Co-Se electrode delivers a higher specific capacitances of 1668, 1632, 1582, 1511, 1442 and 1381 F/g at the current densities of 1, 2, 5, 10, 15 and 20 A/g, respectively. More significantly, when the current density reaches 20 A/g, 82.8% of the initial specific capacitance of the Ni-Co-Se electrode can still be maintained, implying an extremely superior rate capability.

The EIS spectra (Fig. 4e) are investigated to obtain the intrinsic electrochemical conductivity and kinetic mechanisms of the as-fabricated Co-Se, Ni-Co-O and Ni-Co-Se electrode. The impedance spectra at the low-frequency region shows that the Ni-Co-Se electrode delivers a larger linear slope, revealing a lower diffusion limitation during redox reaction, which is related to the superiority of hollow porous nano-architectures. At the high-frequency region (inset in Fig. 4e), Ni-Co-Se electrode delivers smaller series resistance (R_s) and charge transfer resistance (R_{ct}) than those of Co-Se and Ni-Co-O, which are profited from preeminent electrochemical conductivity and charge transfer efficiency by virtue of Ni/Co ionic synergistic contributions and selenylation reaction. Therefore, the EIS results further confirm that Ni-Co-Se with favorable conductivity and reaction activity is a promising electrode material for high-performance supercapacitor.

The cycling stabilities of Co-Se, Ni-Co-O and Ni-Co-Se electrodes are examined *via* continuous GCD measurements for 5000 times at 5 A/g in the potential range of 0 to 0.5 V. The results in Fig. 4f show that the specific capacitances of Co-Se, Ni-Co-O and Ni-Co-Se electrodes are respectively maintained 84.7%, 56.1% and 87.2% of the initial value after 5000 cycles, demonstrating the Ni-Co-Se electrode a good cycling stability. Aforementioned results verify that the as-fabricated Ni-Co-Se electrode possesses outstanding electrochemical properties, which can be attributed to the follow advantages: (i) In general, the infiltration range of electrolyte from the electrode surface to the inside is about 20 nm, meaning that materials with a depth of more than 20 nm have negligible contribution to the electrochemical energy storage. The construction of hollow structure effectively ameliorates this "dead volume" phenomenon and improves the utilization rate of electrode materials [46]; (ii) Hollow Ni-Co-Se structure provides abundant free volume, which effectively alleviates the structural deformation in the process of charge storage (ion/electron transport), thus optimizing the cycle stability of electrode

materials [17]; (iii) The introduction of Ni ions and selenidation increase the specific surface area of the material, shorten the ion/electron transport path, and provide a wealth of active sites for charge storage, which are conducive to the improvement of redox reaction kinetics and conductivity [16].

The flexible all-solid-state hybrid supercapacitor is assembled by employing the Ni-Co-Se positive electrode, AC negative electrode and PVA-KOH hydrogel separator/electrolyte, and assembly mechanism diagram is shown in Fig. 5a. The CV curves of AC and Ni-Co-Se (0-0.7 V) and AC (-1.0–0 V) at 15 mV/s are shown Fig. 5b to determine an appropriate potential window for the as-assembled Ni-Co-Se//AC hybrid supercapacitor. Based on the CV curve, it can be predicted that the appropriate operating voltage window of Ni-Co-Se//AC device is about 0–1.7, and the total capacitances of device are related to the integrated contributions of EDLCs from AC and pseudocapacitance from Ni-Co-Se. Simultaneously, the CV curves of different voltage windows with scanning rate of 10 mV/s are investigated in Fig. 5c. The results show that obvious polarizations occur at 1.6–1.7 V, so 0–1.6 V is selected for the safe operation voltage window.

The CV curves of Ni-Co-Se//AC hybrid supercapacitor in Fig. 5d display the symmetry and negligible peak-shifts with the scan rates increases, manifesting occurrence of fast reversible electrochemical reactions and advantageous rate capability for Ni-Co-Se//AC hybrid supercapacitor. The GCD profiles of the Ni-Co-Se//AC hybrid supercapacitor in Fig. 5e illustrate quasi-isosceles shapes of GCD profiles, demonstrating the reversible electrochemical behavior and good coulombic efficiency for as-assembled supercapacitor device. Moreover, the specific capacitance of Ni-Co-Se//AC hybrid supercapacitor (Fig. 5f) are calculated to be 108.2 F/g at 1 A/g based on the discharge time and operating voltage, and it still retains 90.0 F/g at a high current density of 10 A/g, further verifying the high capacitance and outstanding rate capability of as-assembled supercapacitor. Furthermore, Fig. 5g depicts the corresponding Ragone curve of Ni-Co-Se//AC hybrid supercapacitor calculating from the specific capacitance, voltage/time of discharge and Eqs. 3 and 4. The all-solid-state Ni-Co-Se//AC hybrid supercapacitor delivers a high energy density of 38.5 Wh/kg at a power density of 802.1 W/kg and rate capability (maintained 32.0 Wh/kg at a high power density of 8008.8 W/kg). These remarkable specific energy/power and rate capability are competitive compared to recent similar reports, such as $NiCo_2S_4$//AC [47], $CoSe_2/Ni_{0.85}Se$//AC [42], $CoSe_2$//N-CN [48], *etc.* [30,49–53]. The cyclic stability of the Ni-Co-Se//AC hybrid supercapacitor is

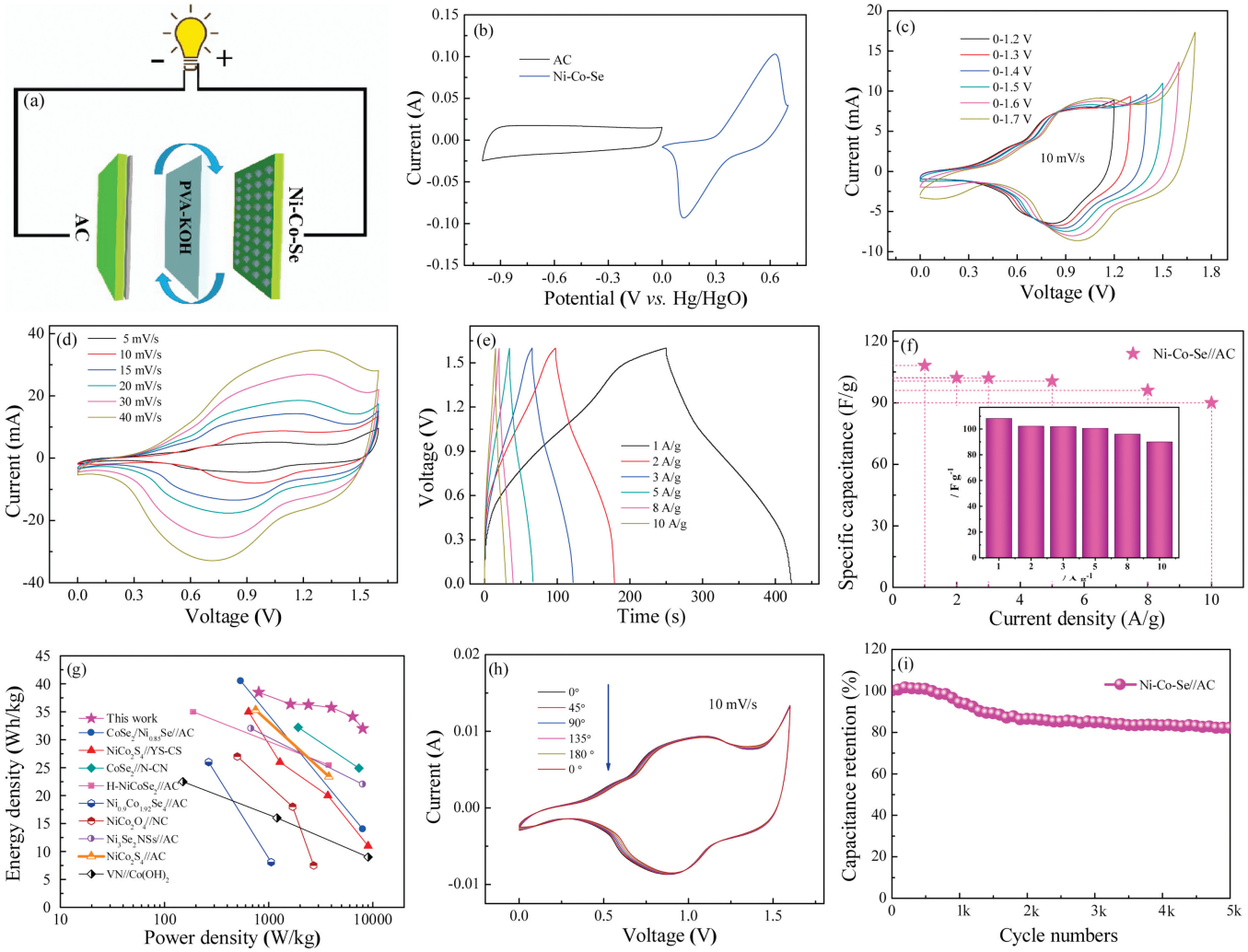

Fig. 5. (a) Schematic illustration of the hybrid supercapacitor based on Ni-Co-Se as the positive electrode and AC as the negative electrode. (b) CV curves of the AC and Ni-Co-Se at 15 mV/s based on three electrode configurations. (c) CV curves of the as-assembled Ni-Co-Se//AC hybrid supercapacitor at 10 mV/s ranging from 1.2 to 1.7 V. (d) CV curves of the as-assembled hybrid supercapacitor with different scan rates in the voltage window of 0–1.6 V. (e) GCD curves of the as-assembled hybrid supercapacitor at different current densities. (f) The corresponding specific capacitances at different current densities. (g) Ragone plot of the as-assembled supercapacitor. (h) The capacitance retention different bending angles at a current density of 10 mV/s. (i) Cycling performance of the assembled supercapacitor at a constant current density of 5 A/g.

evaluated by uninterrupted GCD process at 5 A/g, where the results are revealed in Fig. 5h, and the attenuation of specific capacitance is only 18% of the initial capacitance after 5000 cycles. The mechanical stability of Ni-Co-Se//AC hybrid supercapacitor is subsequently evaluated in Fig. 5i. When the as-assembled device is continuously bent at 0°, 45°, 90°, 135° and 180° at a scanning rate of 10 mV/s, the deformation of the CV curve is almost negligible, indicating that the flexible hybrid supercapacitor based on Ni-Co-Se electrode owns remarkable mechanical robustness, which is not only attributed to the release of stress from the flexible carbon fabric substrates and PVA gel during the bending process, but also PVA gel electrolyte plays a pivotal role in preventing the active materials from falling off and electrolyte leakage [20].

In summary, we are rationally designed and synthesized hollow Ni-Co-Se nano-polyhedron *via* a selenide reaction on ZIF-67. The results demonstrate that Ni-Co-Se electrode possesses high specific capacitance with extraordinary rate performance and favorable cyclic stability, which derive from the particularly structural advantage and the synergistic effect between the bimetallic (Ni/Co) ions. Moreover, the hybrid supercapacitors of Ni-Co-Se//AC display a high energy density of 38.5 Wh/kg at the power density of 802.1 W/kg with a favorable cyclic stability (82.3% of initial capacitance after 5000 cycles) and remarkable mechanical flexibility. Consequently, ZIF-67 derived Ni-Co-Se electrodes are expected to be a candidate for newly smart energy storage devices with high security, stability and flexibility.

Declaration of competing interest

The authors declare that they have no known competing financial interests or personal relationships that could have appeared to influence the work reported in this paper.

Acknowledgments

This work was supported by the National Natural Science Foundation of China (No. 51672109), Natural Science Foundation of Shandong Province for Excellent Young Scholars (No. ZR2016JL015).

Appendix A. Supplementary data

Supplementary material related to this article can be found, in the online version, at doi:https://doi.org/10.1016/j.cclet.2020.01.040.

References

[1] A. Vlad, N. Singh, C. Galande, et al., Adv. Energy Mater. 5 (2015) 1402115.
[2] S. Liu, L. Zheng, P. Yu, et al., Adv. Funct. Mater. 26 (2016) 3331–3339.
[3] L. Liu, C. Du, S. Wang, et al., Chin. Chem. Lett. 29 (2018) 1781–1784.
[4] J. Yang, C. Yu, X. Fan, et al., Energy Environ. Sci. 9 (2016) 1299–1307.
[5] X. Wang, X. Lu, B. Liu, et al., Adv. Mater. 26 (2014) 4763–4782.
[6] W. Zuo, C. Xie, P. Xu, et al., Adv. Mater. 29 (2017) 1703463.
[7] Y. Shao, M.F. El-Kady, J. Sun, et al., Chem. Rev. 118 (2018) 9233–9280.
[8] C. Wang, P. Sun, G. Qu, et al., Chin. Chem. Lett. 29 (2018) 1731–1740.
[9] Q. Zhang, C. Chen, W. Chen, et al., ACS Appl. Mater. Interfaces 11 (2019) 5919–5927.
[10] Y. Jiang, J. Liu, Energy Environ. Mater. 2 (2019) 30–37.
[11] W. Zuo, R. Li, C. Zhou, et al., Adv. Sci. 4 (2017) 1600539.
[12] P. Yu, Z. Zhang, L. Zheng, et al., Adv. Energy Mater. 6 (2016) 1601111.
[13] B. Deng, T. Lei, W. Zhu, et al., Adv. Funct. Mater. 28 (2018) 1704330.
[14] Y. Meng, P. Sun, W. He, et al., Nanoscale 11 (2019) 688–697.
[15] W. He, G. Zhao, P. Sun, et al., Nano Energy 56 (2019) 207–215.
[16] W. He, C. Wang, H. Li, et al., Adv. Energy Mater. 7 (2017) 1700983.
[17] J. Wang, Y. Cui, D. Wang, Adv. Mater. 31 (2019) 1801993.
[18] R. Li, Z. Lin, X. Ba, et al., Nanoscale Horiz. 1 (2016) 150–155.
[19] H.C. Chen, Y. Qin, H. Cao, et al., Energy Storage Mater. 17 (2019) 194–203.
[20] P. Sun, W. He, H. Yang, et al., Nanoscale 10 (2018) 19004–19013.
[21] B. Li, Z. Tian, H. Li, et al., Electrochim. Acta 314 (2019) 32–39.
[22] T. Ma, H. Liu, Y. Wang, et al., Electrochim. Acta 309 (2019) 1–10.
[23] M. Wei, C. Wang, Y. Yao, et al., Chem. Eng. J. 355 (2019) 891–900.
[24] J. Balamurugan, C. Li, V. Aravindan, et al., Adv. Funct. Mater. 28 (2018) 1803287.
[25] P. Ge, S. Li, L. Xu, et al., Adv. Energy Mater. 9 (2019) 1803035.
[26] P. Ge, C. Zhang, H. Hou, et al., Nano Energy 48 (2018) 617–629.
[27] X.-F. Lu, D.-J. Wu, R.-Z. Li, et al., J. Mater. Chem. A 2 (2014) 4706–4713.
[28] A. Indra, T. Song, U. Paik, Adv. Mater. 30 (2018) 1705146.
[29] Y. Li, X. Liu, H. Li, et al., J. Power Sources 422 (2019) 122–130.
[30] Q. Wang, F. Gao, B. Xu, et al., Chem. Eng. J. 327 (2017) 387–396.
[31] K. Yang, Y. Yan, W. Chen, et al., J. Electroanal. Chem. 851 (2019) 113445.
[32] Q. Shi, Z. Chen, Z. Song, et al., Angew. Chem. Int. Ed. 50 (2011) 672–675.
[33] C. Xia, Q. Jiang, C. Zhao, et al., Nano Energy 24 (2016) 78–86.
[34] P. Sun, C. Wang, W. He, et al., ACS Sustain. Chem. Eng. 5 (2017) 10139–10147.
[35] Q. Jiang, N. Kurra, M. Alhabeb, et al., Adv. Energy Mater. 8 (2018) 1703043.
[36] S.-K. Park, J.K. Kim, Y. Chan Kang, J. Mater. Chem. A 5 (2017) 18823–18830.
[37] J.S. Cho, S.Y. Lee, Y.C. Kang, Sci. Rep. 6 (2016) 23338.
[38] F. Gong, X. Xu, Z. Li, et al., Chem.Commun. 49 (2013) 1437–1439.
[39] I.H. Kwak, H.S. Im, M.J. Dong, et al., ACS Appl. Mater. Interfaces 8 (2016) 5327.
[40] C. Wang, K. Guo, W. He, et al., Sci. Bull. 62 (2017) 1122–1131.
[41] M.C. Biesinger, B.P. Payne, A.P. Grosvenor, et al., Appl. Surf. Sci. 257 (2011) 2717–2730.
[42] J. Lin, H. Wang, Y. Yan, et al., J. Mater. Chem. A 6 (2018) 19151–19158.
[43] J.K. Kim, G.D. Park, J.H. Kim, et al., Small 13 (2017) 1700068.
[44] Y. Chen, Z. Ren, H. Fu, et al., Small 14 (2018) 1800763.
[45] Q. Lu, J.G. Chen, J.Q. Xiao, Angew. Chem. Int. Ed. 52 (2013) 1882–1889.
[46] X.F. Lu, A.L. Wang, H. Xu, et al., J. Mater. Chem. A 3 (2015) 16560–16566.
[47] P. Cai, T. Liu, L. Zhang, et al., Appl. Surf. Sci. 504 (2020) 144501.
[48] T. Chen, S. Li, J. Wen, et al., Small 14 (2018) 1700979.
[49] G. Nagaraju, S.M. Cha, S.C. Sekhar, et al., Adv. Energy Mater. 7 (2017) 1601362.
[50] C. Guan, X. Liu, W. Ren, et al., Rational Adv. Energy Mater. 7 (2017) 1602391.
[51] L. Hou, Y. Shi, C. Wu, et al., Adv. Funct. Mater. 28 (2018) 1705921.
[52] R. Wang, X. Yan, J. Lang, et al., J. Mater. Chem. A 2 (2014) 12724–12732.
[53] W. An, L. Liu, Y. Gao, et al., RSC Adv. 6 (2016) 75251–75257.